Electric field dependence of optical phonon frequencies in wurtzite GaN observed in GaN high electron mobility transistors

Citation: Bagnall, Kevin R.; Dreyer, Cyrus E.; Vanderbilt, David et al. "Electric Field Dependence of Optical Phonon Frequencies in Wurtzite GaN Observed in GaN High Electron Mobility Transistors." Journal of Applied Physics 120, 15 (October 2016): 155104

As Published: http://dx.doi.org/10.1063/1.4964689

Publisher: American Institute of Physics (AIP)

Persistent URL: http://hdl.handle.net/1721.1/110800

Version: Author's final manuscript: final author's manuscript post peer review, without publisher's formatting or copy editing

Electric Field Dependence of Optical Phonon Frequencies in Wurtzite GaN Observed in GaN High Electron Mobility Transistors

Kevin R. Bagnall[1], Cyrus E. Dreyer[2], David Vanderbilt[2], and Evelyn N. Wang[1]

[1]Department of Mechanical Engineering, Massachusetts Institute of Technology, Cambridge, MA 02139, USA
[2]Department of Physics and Astronomy, Rutgers, the State University of New Jersey, Piscataway, NJ 08854-8019, USA

October 19, 2016

Abstract

Due to the high dissipated power densities in gallium nitride (GaN) high electron mobility transistors (HEMTs), temperature measurement techniques with high spatial resolution, such as micro-Raman thermography, are critical for ensuring device reliability. However, accurately determining the temperature rise in the ON state of a transistor from shifts in the Raman peak positions requires careful decoupling of the simultaneous effects of temperature, stress, strain, and electric field on the optical phonon frequencies. Although it is well-known that the vertical electric field in the GaN epilayers can shift the Raman peak positions through the strain and/or stress induced by the inverse piezoelectric (IPE) effect, previous studies have not shown quantitative agreement between the strain and/or stress components derived from micro-Raman measurements and those predicted by electro-mechanical models. We attribute this discrepancy to the fact that previous studies have not considered the impact of the electric field on the optical phonon frequencies of wurtzite GaN apart from the IPE effect, which results from changes in the atomic coordinates within the crystal basis and in the electronic configuration. Using density functional theory, we calculated the zone center E_2 (high), A_1 (LO), and E_2 (low) modes to shift by -1.39 cm^{-1}/(MV/cm), 2.16 cm^{-1}/(MV/cm), and -0.36 cm^{-1}/(MV/cm) respectively, due to an electric field component along the *c*-axis, which are an order of magnitude larger than the shifts associated with

the IPE effect. Then, we measured changes in the E_2 (high) and A_1 (LO) Raman peak positions with ≈1 μm spatial resolution in GaN HEMTs biased in the pinched OFF state and showed good agreement between the strain, stress, and electric field components derived from the measurements and our 3D electro-mechanical model. This study helps to explain the reason the pinched OFF state is a suitable reference for removing the contributions of the electric field and the IPE-induced stress from the temperature rise in the ON state and suggests that the IPE-induced stress in the GaN buffer is an order of magnitude smaller than previously believed. Our analysis and experimental results support previous theoretical studies discussing the electric field dependence of optical phonon frequencies apart from the IPE effect and suggest this is a general phenomenon occurring in all wurtzite and zincblende crystals. The total electric field dependence of the optical phonon frequencies in piezoelectric crystals is a critical consideration in accurately characterizing the stress, strain, electric field, and temperature distributions in microelectronic devices *via* micro-Raman spectroscopy.

I. Introduction

Over the last fifteen years, gallium nitride (GaN) high electron mobility transistors (HEMTs) have become a promising compound semiconductor technology for both high voltage power conversion and high power wireless communication applications [1]-[2]. However, the dissipated power density levels present in GaN HEMTs often lead to elevated channel temperatures, which need to be properly characterized and managed to ensure device lifetime and reliability. Due to its high spatial and temporal resolution, micro-Raman thermography has emerged as one of the most popular techniques for measuring local temperature rise in GaN HEMTs [3]-[7]. Determination of the device temperature from changes in the Raman peak

positions (associated with the Stokes or phonon emission process) requires properly accounting for mechanical stresses induced by the thermoelastic [4]-[6] and inverse piezoelectric (IPE) effects [8]-[10]. The most common practice in the literature to achieve this is to measure the changes in Raman peak positions of the E_2 (high) and/or A_1 (LO) modes between the pinched OFF state ($V_{gs} = V_g - V_s < V_{th}$) and the ON state ($V_{gs} > V_{th}$) at the same drain bias ($V_{ds} = V_d - V_s > 0$), where V_d, V_g, and V_s are the voltages of the drain, gate, and source contacts, respectively, and V_{th} is the gate threshold voltage. A schematic of a typical lateral GaN HEMT layout grown on a foreign substrate with an aluminum gallium nitride (AlGaN) barrier and that of the micro-Raman thermography methodology are shown in Figure 1.

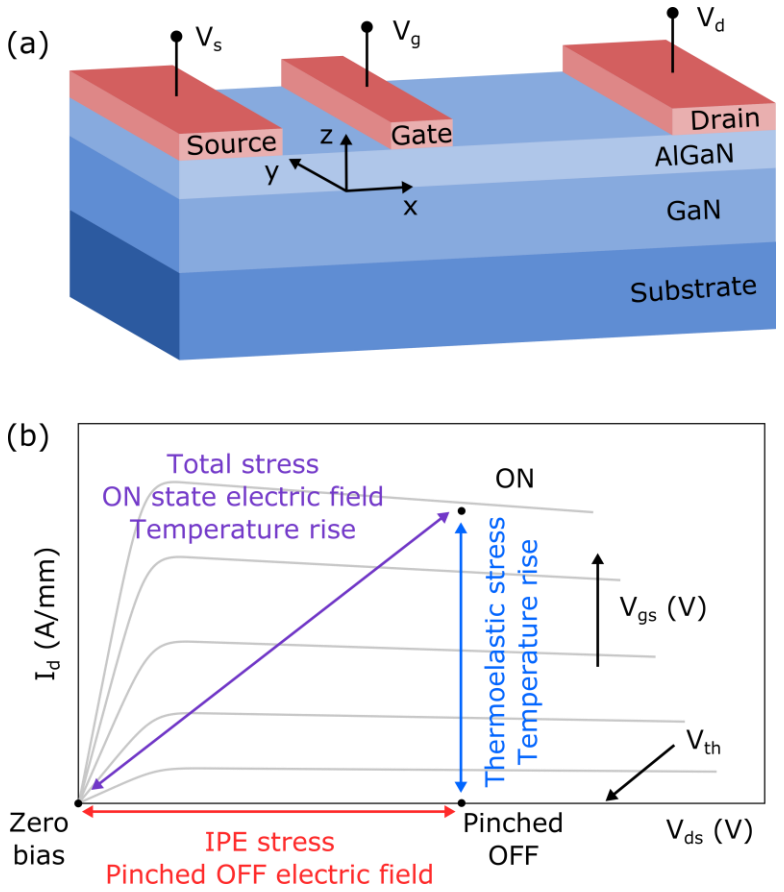

FIG. 1. Schematics of (a) a lateral GaN HEMT structure and (b) the drain current-voltage ($I_d - V_{ds}$) output characteristics with the contributions of stress, electric field, and temperature to the change in Raman peak positions. The drain and gate biases are referenced with respect to the source, i.e., $V_{ds} = V_d - V_s$ and $V_{gs} = V_g - V_s$. The gate threshold voltage V_{th} is the gate bias below which there is negligible drain current ($\lesssim$1 mA/mm).

From the basic operating principles of a GaN HEMT, the application of a positive drain bias in the pinched OFF state and in the ON state should induce a negative electric field component along the z-axis in the GaN buffer in the gate-drain access region and under the drain contact. Because the temperature rise in the pinched OFF state is negligible and the average electric field component along the z-axis in the GaN buffer is primarily a function of the drain bias, the difference in Raman peak position between the pinched OFF state and the ON state should not include the contributions of the IPE-induced stress and the vertical electric field [8],[10]. Thus, the

temperature rise and thermoelastic stress can be simultaneously determined from changes in the positions of two Raman peaks between these two bias conditions [5]-[6]. Despite the success of using the pinched OFF state as the unpowered reference for micro-Raman temperature measurements that agree with thermal models and micro-Raman measurements based on the Stokes/anti-Stokes ratio (which should not be affected by strain, stress, and electric field), there has been considerable difficulty in deriving quantitative values of the IPE-induced strain and stress components from micro-Raman measurements that agree with electro-mechanical models [8]-[10]. Analysis of the Raman peak shifts of the E_2 (high) and A_1 (LO) modes between the zero bias state (V_{ds} = 0 and V_{gs} = 0) and the pinched OFF state based on potential deformation theory and linear piezoelasticity leads to contradictions in the sign and order of magnitude of the strain, stress, and electric field components predicted by simple physical arguments and rigorous electro-mechanical modeling [8]-[10].

Several hypotheses, such as uncertainties in the piezoelectric properties or phonon deformation potentials of GaN, have been suggested to explain the significant disagreement between measured and modeled values of strain, stress, and electric field [8]-[10],[11]. Our recent review [10] investigated many of these hypotheses in detail and concluded that none of them can satisfactorily resolve this disagreement. In this work, we show that the source of the discrepancy is the fact that the electric field also affects the internal structural parameters of wurtzite GaN beyond the macroscopic strain induced by the IPE effect. We calculated the magnitude of the phonon frequency shift with electric field along the c-axis for the E_2 (high), A_1 (LO), and E_2 (low) modes at the Γ-point via density functional theory (DFT). To substantiate this theory, we measured changes in the Raman peak positions of these modes in GaN HEMTs biased in the pinched OFF state and showed good quantitative agreement with the correct sign and order of magnitude

between measured and modeled values of strain, stress, and electric field. These measurements that quantify the electro-mechanical state of the GaN buffer directly support the use of the pinched OFF state as the proper reference for micro-Raman thermometry of GaN HEMTs. In a more general sense, our results also indicate that the non-IPE contribution to optical phonon frequency shifts of polar semiconductors in an electric field should always be present and may be more significant than the IPE strain-related contribution.

II. Theory

A. Optical Phonon Frequency Shifts with Strain

Wurtzite GaN is a hexagonal crystal with C_{6v} (6mm) point group symmetry and a four atom basis as shown in Figure 2. The lattice parameters a and c define the size of the primitive unit cell and are related to the macroscopic deformation of the crystal, i.e., the strain components, through the relations

$$\epsilon_{xx} = \epsilon_{yy} = \frac{a - a_0}{a_0} \tag{1a}$$

$$\epsilon_{zz} = \frac{c - c_0}{c_0} \tag{1b}$$

where a_0 and c_0 are the equilibrium values of the lattice constants. The internal structural r parameter is the bond length between the Ga and N atoms along the c-axis and defines the internal coordinates of the atoms in the basis together with a and c. In the typical Ga-face grown GaN epilayers, the c-axis corresponding to the direction from the Ga atom to the nearest N atom above it along the c-direction is the positive z-axis by convention [12]. Thus, the positive z-axis of the coordinate system for GaN HEMTs in this work was chosen to point in the direction from the

substrate to the barrier. The x- and y-axes were chosen to be the directions along the channel from the source to the drain and along the gate, respectively, which correspond to mutually orthogonal directions in the c-plane.

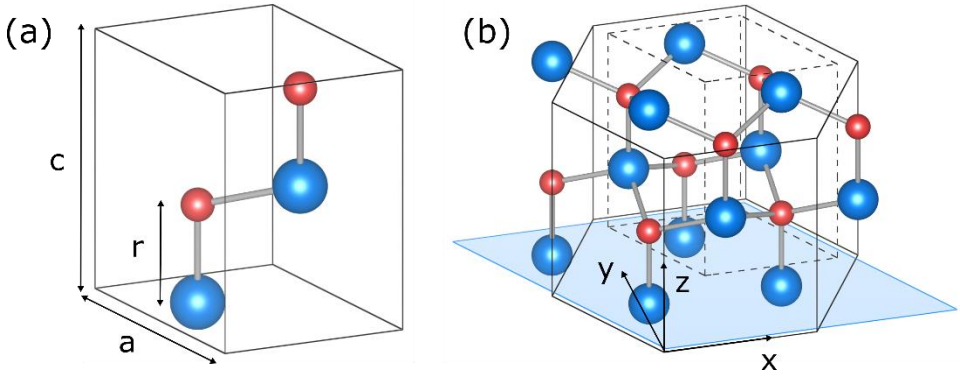

FIG. 2. (a) Wurtzite GaN unit cell and (b) crystal structure in which larger blue and smaller red spheres denote Ga and N atoms, respectively. Crystal structures were drawn with the VESTA visualization software [13].

Due to the negative electric field component along the c-axis of the GaN buffer, the linear IPE effect predicts that the buffer will experience a combination of strain and stress related by the constitutive relation

$$\epsilon_{ij} = S_{ijk\ell}\sigma_{k\ell} + d_{kij}E_k \tag{2}$$

where ϵ_{ij} is the strain tensor, $S_{ijk\ell}$ is the elastic susceptibility tensor, $\sigma_{k\ell}$ is the stress tensor, d_{kij} is the piezoelectric modulus tensor, and E_k is the electric field vector [14]. The strain induced by the IPE effect changes the interatomic distances and force constants, resulting in changes in the optical phonon frequencies of the crystal. By probing the optical phonon frequencies near the Γ-point, micro-Raman spectroscopy can be used to experimentally measure this IPE-induced strain in GaN HEMTs with ≈1 μm spatial resolution from changes in the Raman peak positions [8]-[10]. Raman selection rules specify that only the E_2 (high), A_1 (LO), and E_2 (low) modes can be observed

in the backscattering $\bar{z}(\cdot\cdot)z$ configuration, which is most suitable for the lateral GaN HEMT structure [15]. Figure 3 shows a schematic of these modes indicating the relative motion of the four atoms in the basis along with a representative Raman spectrum of the GaN buffer on a silicon carbide (SiC) substrate.

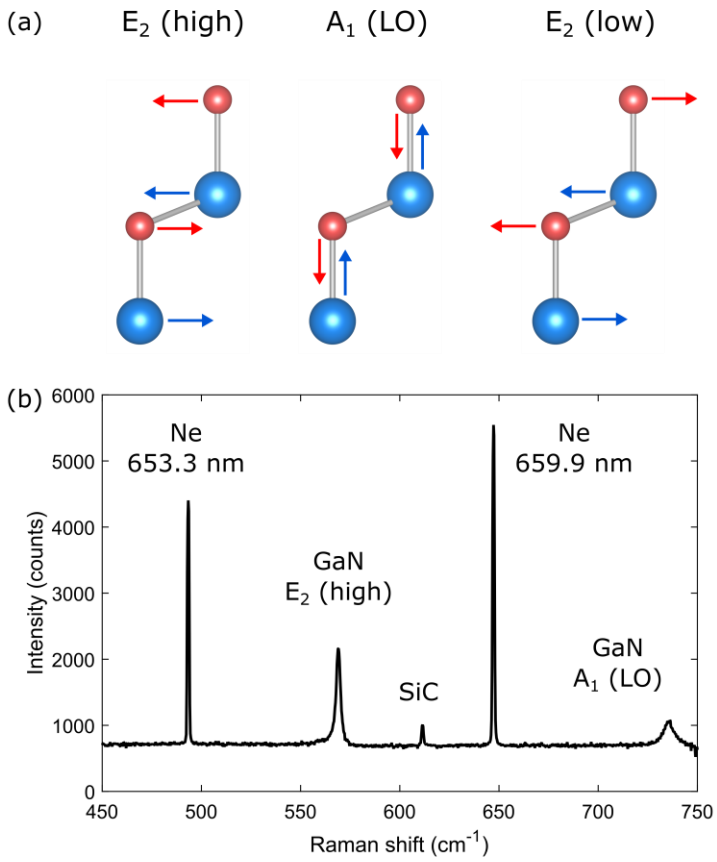

FIG. 3. (a) Relative motion of the atoms for the E_2 (high), A_1 (LO), and E_2 (low) optical modes of wurtzite GaN and (b) representative Raman spectrum showing the E_2 (high) and A_1 (LO) peaks along with spontaneous emission lines of neon (Ne) used to calibrate the spectrum [16].

Linear potential deformation theory [17], which combines group theory and first-order perturbation theory, predicts how the frequencies of the optical phonon modes shift with macroscopic strain by expanding the perturbation to the crystal potential in terms of the strain

components. Due to the symmetry properties of the strain tensor and those of the E_2 and A_1 optical modes in the point group C_{6v}, the first-order changes in frequency of these modes are related to specific strain components by the relations

$$\Delta\omega_{E_2}^{(i)} = a_{E_2}(\epsilon_{xx} + \epsilon_{yy}) + b_{E_2}\epsilon_{zz} \pm c_{E_2}\sqrt{(\epsilon_{xx} - \epsilon_{yy})^2 + 4\epsilon_{xy}^2} \tag{3a}$$

$$\Delta\omega_{A_1}^{(i)} = a_{A_1}(\epsilon_{xx} + \epsilon_{yy}) + b_{A_1}\epsilon_{zz} \tag{3b}$$

where a_n, b_n, and c_n are strain the phonon deformation potentials (PDPs) of each mode (not to be confused with the lattice parameters a and c). By substituting the constitutive relation in Equation (2) into Equation (3a), the frequency shift of the E_2 (high) mode can be equivalently written in terms of the stress and electric field components as

$$\begin{aligned}\Delta\omega_{E_2}^{(i)} = {} & \left[a_{E_2}(S_{11} + S_{12}) + b_{E_2}S_{13}\right](\sigma_{xx} + \sigma_{yy}) + \left[2a_{E_2}S_{13} + b_{E_2}S_{33}\right]\sigma_{zz} \\ & \pm c_{E_2}|S_{11} - S_{12}|\sqrt{(\sigma_{xx} - \sigma_{yy})^2 + 4\sigma_{xy}^2} + \left[2a_{E_2}d_{31} + b_{E_2}d_{33}\right]E_z\end{aligned} \tag{4}$$

The corresponding shift in the A_1 (LO) frequency in terms of the stress and electric field components is identical to Equation (4) except for the omission of the third term.

Consideration of the mechanical boundary conditions imposed on the GaN buffer allows one to further simplify Equation (4) in the pinched OFF state in GaN HEMTs. Mechanical clamping on the bottom surface of the buffer by the substrate and free expansion of the top surface of the buffer results in negligible stress along the c-axis compared to that in the c-plane ($|\sigma_{zz}| \ll |\sigma_{xx}|$), negligible strain in the c-plane compared to that along the c-axis ($|\epsilon_{xx}| \ll |\epsilon_{zz}|$), and approximate symmetry in the c-plane ($\epsilon_{xx} \approx \epsilon_{yy}$ and $\sigma_{xx} \approx \sigma_{yy}$) [10]. From the sign of the electric field component along the c-axis ($E_z < 0$), one finds that the strain along the c-plane is expected

to be negative ($\epsilon_{zz} < 0$) and the stress in the c-plane is expected to be negative or compressive ($\sigma_{xx} < 0$). Despite knowing values of the elastic and piezoelectric constants and strain PDPs of wurtzite GaN with reasonable certainty, there have been serious discrepancies in the sign and order of magnitude of the strain, stress, and electric field components derived from measured shifts of the E_2 (high) and A_1 (LO) Raman peaks and those predicted by electro-mechanical modeling of GaN HEMTs [8]-[10]. We attribute this discrepancy to the fact that Equations (3a) to (4) are missing an important contribution of the electric field to the frequency shifts apart from the IPE effect.

B. Optical Phonon Frequency Shifts with Electric Field

As described by Wang and Vanderbilt [18], an electric field can shift the phonon frequencies of an electrical insulator by three mechanisms: (i) a change in the lattice constants, which is described by the macroscopic strain induced by the IPE effect, (ii) a change in the atomic coordinates within the crystal basis, and (iii) a change in the electron configuration, which influences the phonon frequencies through electron-phonon coupling. Based on these insights and the principle that two independent, intensive properties (strain, stress, electric field, or polarization) are required to specify the thermodynamic state of a piezoelectric crystal [14], the perturbation to the crystal potential in the presence of an electric field must contain two independent terms involving the strain and electric field

$$V = \sum_{ij} V_{ij}^{(i)} \epsilon_{ij} + \sum_{k} V_{k}^{(ii+iii)} E_k \tag{5}$$

The form of Equation (5) is particularly useful because it simply adds a correction term to the standard formalism of potential deformation theory based on strain alone given by Equations (3a) to (4) and corresponds to the effects described by Wang and Vanderbilt [18]. In the Appendix, we

show that the second term in Equation (5) results in an additional term that needs to be added to Equations (3a), (3b), and (4) to account for the phonon frequency shifts with the vertical electric field component E_z. This is also consistent with the analysis by Ganesan *et al.* [19], who proposed that the optical phonon frequencies in crystals without inversion symmetry should change linearly with the electric field apart from IPE-induced strain. Although non-zero lateral electric field components E_x and E_y are present in the GaN buffer in the pinched OFF state, their effect on the E_2 (high) and A_1 (LO) mode frequencies is a second-order one whose magnitude is much smaller than the first-order contribution of E_z. Assuming free expansion of the GaN buffer along the c-axis ($\sigma_{zz} = 0$), symmetric stress in the c-plane ($\sigma_{xx} = \sigma_{yy}$), negligible shear stress in the c-plane ($\sigma_{xy} = 0$), the total frequency shift of the E_2 (high) and A_1 (LO) modes is given by

$$\begin{aligned} \Delta\omega_n &= \Delta\omega_n^{(i)} + \Delta\omega_n^{(ii+iii)} \\ &= K_n^{II}\sigma_{xx} + \left[B_n^{(i)} + B_n^{(ii+iii)}\right]E_z \\ &= K_n^{II}\sigma_{xx} + B_n E_z \end{aligned} \tag{6}$$

where $K_n^{II} = 2a_n(S_{11} + S_{12}) + 2b_n S_{13}$ is the biaxial stress coefficient, $B_n^{(i)} = 2a_n d_{13} + b_n d_{33}$ the electric field coefficient due to the IPE effect, $B_n^{(ii+iii)}$ is the electric field coefficient apart from the IPE effect, and B_n is the total electric field coefficient.

The existence and importance of the $B_n^{(ii+iii)}$ coefficient can also be derived by considering the changes in the lattice parameters a and c and the internal structural r parameter (or $u = r/c$) in the presence of an electric field $\vec{E} = E_z\hat{z}$ along the c-axis. If the symmetry of the wurtzite structure is preserved under the perturbation of the strain tensor ϵ_{ij} and the electric field E_k, the crystal structure is still fully defined by a, c, and u. If there are no constraints on the expansion of the crystal (zero stress), the normal strain components are given by $\epsilon_{xx} = \epsilon_{yy} = d_{31}E_z$ and $\epsilon_{zz} =$

$d_{33}E_z$, which signify changes in the lattice parameters a and c with the electric field. As the lattice parameters change, the internal structural u parameter does not remain constant. Rather, the u parameter must also change by

$$\begin{aligned}\Delta u^{(i)} &= u^{(i)} - u_0 = \frac{\partial u^{(i)}}{\partial a}\Delta a + \frac{\partial u^{(i)}}{\partial c}\Delta c \\ &= \left[\frac{\partial u^{(i)}}{\partial a}a_0 d_{31} + \frac{\partial u^{(i)}}{\partial c}c_0 d_{33}\right]E_z = \frac{\partial u^{(i)}}{\partial E_z}E_z\end{aligned} \tag{7}$$

to minimize the total energy of the crystal, where $\frac{\partial u^{(i)}}{\partial a}$ and $\frac{\partial u^{(i)}}{\partial c}$ are the rates of change of u with the lattice parameters a and c, respectively. This description of the response of the crystal to an electric field E_z is consistent with Equations (3a) and (3b) and the effect of type (i) discussed by Wang and Vanderbilt [18]. If the crystal were rigidly clamped so that the lattice parameters a and c did not change in the presence of a vertical electric field E_z, Equations (2) to (4) and (7) suggest that the macroscopic strain components ϵ_{xx}, ϵ_{yy}, and ϵ_{zz}, the internal strain component $\Delta u^{(i)}/u_0$, and the phonon frequency shifts would be zero

However, it is important not to neglect the possibility of the internal structural u parameter changing in the presence of a vertical electric field E_z while the lattice parameters a and c remain constant (zero macroscopic strain). Owing to the fact that the Ga-N bond in wurtzite GaN is strongly polar, the Ga and N ions assume positive and negative ionic charges, respectively, that result in an electric dipole along the Ga-N bond. In the presence of a vertical electric field, one would expect the bond length r and internal structural u parameter to lengthen or shorten depending on the direction of the field relative to that of the dipole. This type (ii) effect related to the change in internal atomic coordinates within the basis and the type (iii) effect associated with electron-phonon coupling can be captured to first-order in the electric field by the Born effective

charge tensor Z_{ij}^{α}, which describes the force $F_i^{\alpha} = Z_{ij}^{\alpha} E_j$ on atom α in the ith direction due to an electric field component in the jth direction. This extra force displaces each atom β by an amount ΔR_j^{β} in the direction j from its $\vec{E} = 0$ equilibrium position as determined by the system of equations

$$Z_{ij}^{\alpha} E_j - \sum_{\beta} C_{ij}^{\alpha\beta} \Delta R_j^{\beta} = 0 \tag{8}$$

where $C_{ij}^{\alpha\beta}$ are the interatomic force constants (IFCs) describing the force on atom α in the ith direction when atom β is displaced in the jth direction. Because the perturbation E_z transforms as the fully symmetric representation A_1 in the point group C_{6v}, symmetry analysis indicates that the resulting atomic displacements ΔR_j^{β} should also transform as A_1. Since this deformation is not associated with macroscopic strain (corresponding to the A_1 acoustic phonon mode), the relative change in positions of the atoms is identical to that of the A_1 optical phonon modes, in which the u parameter changes by the Ga and N atoms being displaced in opposite directions.

To connect this microscopic picture to the phonon frequency shifts predicted by the more general potential deformation theory developed in Equations (5) and (6), the phonon frequency shift of mode n can be written as a series expansion in the lattice parameters a and c and the internal structural u parameter as

$$\begin{aligned} \Delta\omega_n &= \left.\frac{\partial \omega_n}{\partial a}\right|_{u,c} \Delta a + \left.\frac{\partial \omega_n}{\partial c}\right|_{u,a} \Delta c + \frac{\partial \omega_n}{\partial u^{(i)}} \Delta u^{(i)} + \left.\frac{\partial \omega_n}{\partial u^{(ii+iii)}}\right|_{a,c} \Delta u^{(ii+iii)} \\ &= 2a_n \epsilon_{xx} + b_n \epsilon_{zz} + \left.\frac{\partial \omega_n}{\partial u^{(ii+iii)}}\right|_{a,c} \Delta u^{(ii+iii)} \\ &= 2a_n \epsilon_{xx} + b_n \epsilon_{zz} + B_n^{(ii+iii)} E_z \end{aligned} \tag{9}$$

where we have explicitly separated the change in ω_n associated with changes in the u parameter due to the effects of type (i), (ii), and (iii). Equation (9) is identical to Equations (3a) and (3b) augmented by the term $B_n^{(ii+iii)}E_z$ under the simplification of symmetric normal strain in the c-plane. In summary, this analysis shows that the internal structural u parameter can change independently of the macroscopic strain and that the total phonon frequency shift with stress and electric field should include a term that is independent of the IPE effect. To the best of our knowledge, numerical values of the electric field coefficient $B_n^{(ii+iii)}$ have never been reported for the optical phonon modes of wurtzite GaN. Including terms associated with effects of type (ii) and (iii) in Equations (6) and (9), such as $\Delta\omega_n^{(ii+iii)} = B_n^{(ii+iii)}E_z$, is actually required to determine the effect of an electric field on the phonon frequencies of any piezoelectric crystal, which we describe in more detail in the Appendix. Depending upon the point group of the crystal, terms associated with the other electric field components E_x and E_y may also be present.

III. First Principles Calculations

To predict the magnitude of the electric field coefficient $B_n^{(ii+iii)}$, we first calculated the Born effective charges, IFCs, and zone center phonon frequencies for the four atom wurtzite GaN unit cell at zero electric field via DFT with the HSE hybrid functional [20] and PAW pseudopotentials [21] implemented in the VASP [22]. For the Ga PAW potential, the semi-core *d* electrons were frozen in the core; tests with Ga *d* electrons treated in the valence indicated that our conclusions were unaffected. The HSE mixing parameter was set to α = 0.31 to provide accurate structural parameters, and the screening parameter was set to its default value of ω = 0.2. A plane wave energy cutoff of 600 eV and a Γ-centered Monkhorst-Pack [23] k-point mesh of 6 × 6 × 4 were used. Convergence tests with higher cutoffs (up to 800 eV) and more k points (up to 8 × 8

× 6) indicated that the phonon frequencies had converged to within ≈3 cm^{-1}. Non-analytic corrections for the frequencies at Γ were applied with the PHONOPY package [24]. The changes in equilibrium positions of the atoms at a non-zero electric field along the c-axis were computed with Equation (8) and the zero field Born effective charges and IFCs, which amounts to a first order treatment of the ionic and electronic response to the electric field [18],[25]. The zone center phonon frequencies were then re-calculated at the new equilibrium atomic positions, resulting in phonon frequencies that varied linearly with the applied electric field. The HSE functional was found to give accurate phonon frequencies at zero electric field though calculations with semilocal functionals gave trends of frequency versus E_z to within 15% of the HSE functional. We have also confirmed that the use of the Born effective charges and IFCs calculated at $E_z = 0$ accurately models the true electric field displacements for $E_z \neq 0$ with calculations using the finite electric field implementation in the ABINIT code [26].

From our DFT calculations, we found that the internal structural u parameter changes with the lattice parameters by $\frac{\partial u^{(i)}}{\partial a}$ = 0.0565 $Å^{-1}$ and $\frac{\partial u^{(i)}}{\partial c}$ = -0.035 $Å^{-1}$ when a macroscopic strain is imposed on the crystal. Using equilibrium values of the lattice constants a_0 = 3.1878 Å and c_0 = 5.185 Å [27] and piezoelectric moduli d_{31} = -1.37 × 10^{-4} cm/MV and d_{33} = 2.83 × 10^{-4} cm/MV [28] in Equation (7), the corresponding rate of change of u with the field E_z associated with the IPE-induced strain is $\frac{\partial u^{(i)}}{\partial E_z}$ = -7.6 × 10^{-5} cm/MV. The rate of change of the u parameter with the vertical electric field at fixed values of a and c, however, is an order of magnitude larger with a value of $\frac{\partial u^{(ii+iii)}}{\partial E_z}$ = -4.8 × 10^{-4} cm/MV. This strong dependence of the u parameter on the vertical electric field E_z at zero macroscopic strain shortens and stiffens the Ga-N bond along the c-axis and significantly increases the frequency of the A_1 (LO) mode. In contrast, the Ga-N bond length

in the c-plane increases, resulting in a decrease in frequency of both the E_2 (low) and E_2 (high) modes. Figure 4 shows the shift in phonon frequencies with electric field along the c-axis with schematics of the atomic displacements in the inset.

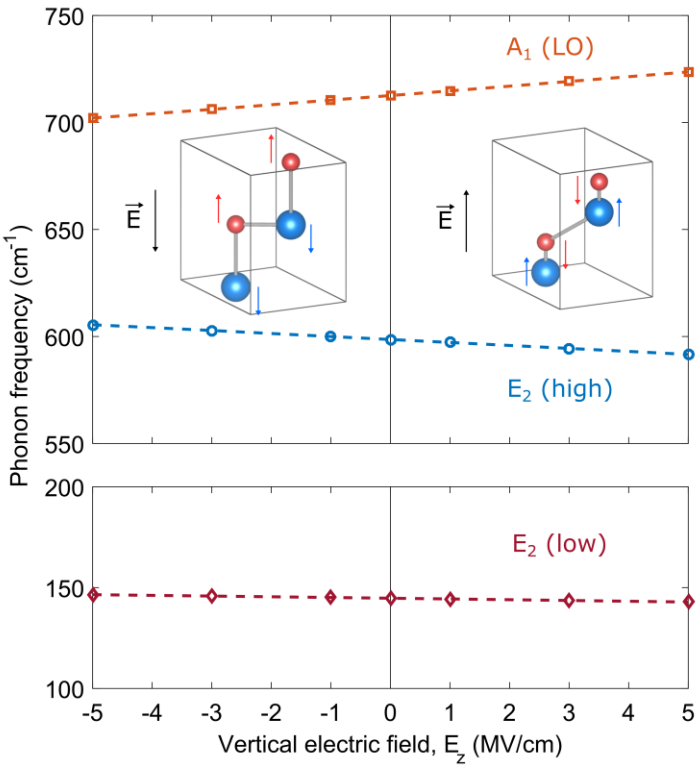

FIG. 4. Phonon frequency shifts of the E_2 (high), A_1 (LO), and E_2 (low) modes of wurtzite GaN with electric field along the c-axis. Inset schematic shows the change in atomic positions within the unit cell due to the vertical electric field.

The resulting electric field coefficients $B_n^{(ii+iii)}$ are significantly higher than the coefficients $B_n^{(i)}$ associated with the IPE effect alone, especially for the E_2 (high) and A_1 (LO) modes. In Table I, we provide values of the biaxial stress and electric field coefficients for the E_2 (high), A_1 (LO), and E_2 (low) modes taken or derived from references in the literature and our calculations in this work. For the E_2 (high) and A_1 (LO) modes, we used the biaxial stress coefficients measured by Choi *et al.* [27] from the residual stress in GaN epilayers adjusted with

recently reported values of the elastic constants [28]. For the E_2 (low) mode, we used the biaxial stress coefficient calculated from the hydrostatic and uniaxial stress coefficients reported by different groups [29]-[30]. To determine the IPE-related electric field coefficient, we used the strain PDPs (a_{E_2H} = -923 cm^{-1}, b_{E_2H} = -856 cm^{-1}, a_{A_1LO} = -753 cm^{-1}, b_{A_1LO} = -1117 cm^{-1}, a_{E_2L} = 197 cm^{-1}, and b_{E_2L} = -208 cm^{-1}) from different references [27],[29]-[30] and the elastic constants and piezoelectric moduli d_{31} = -1.37 pm/V and d_{33} = 2.83 pm/V measured on bulk ammonothermal GaN crystals [28].

TABLE I. Biaxial stress and vertical electric field coefficients of the zone center optical phonon frequencies for the E_2 (high), A_1 (LO), and E_2 (low) modes of wurtzite GaN.

Mode	K^{II} (cm^{-1}/GPa)	$B^{(i)}$ cm^{-1}/(MV/cm)	$B^{(ii+iii)}$ cm^{-1}/(MV/cm)
E_2 (high)	-3.14[a]	0.01[c]	-1.39
A_1 (LO)	-2.11[a]	-0.11[c]	2.16
E_2 (low)	1.09[b]	-0.11[c]	-0.36

a. Ref. [27] adjusted with the elastic constants from Ref. [28].
b. Refs. [29]-[30].
c. Calculated from Refs. [27]-[30].

III. Experimental Technique

To demonstrate this effect experimentally in GaN HEMTs, we measured changes in the E_2 (high), A_1 (LO) and E_2 (low) Raman peak positions of commercially available GaN on SiC HEMTs (CGHV1J006D, Cree) designed for RF power amplifier applications. These 6 × 200 µm HEMTs consisted of a 22 nm $Al_{0.22}Ga_{0.78}N$ barrier, 1.4 µm insulating GaN buffer, and 100 µm SiC substrate with a gate length of L_g = 0.25 µm and gate-drain spacing of L_{gd} = 3.7 µm [31]. Raman spectra of the GaN buffer were acquired in the backscattering configuration with a free space micro-Raman

spectroscopy system consisting of a 632.904 nm frequency stabilized diode laser (SLM-FS, REO), optical microscope (BX41, Olympus), long pass edge filter (LP02-633RU-25, Semrock), and 750 mm focal length spectrograph (Acton Spectra-Pro SP-2750, Princeton Instruments) equipped with a 1800 lines/mm grating and CCD camera (PIXIS 400 BR, Princeton Instruments). A 100× microscope objective with a numerical aperture of 0.8 (LMPlanFL N, Olympus) was used to focus the laser excitation and collect the Raman scattered light, resulting in a laser spot of size of ≈1.0 μm and depth of field of ≈4 μm [32]. Each Raman spectrum was individually calibrated with spontaneous emission lines from a neon calibration lamp (6032, Newport) to provide high precision and repeatability [16]. The temperature of the device was maintained at 20.0 ± 0.1 °C by a thermoelectric cooling module to eliminate the possible effect of temperature changes on the Raman peak positions.

Under the simplifying approximations of symmetric stress and strain in the c-plane, negligible shear stress in the c-plane, and negligible stress along the c-axis, the frequency shifts of the E_2 (high), A_1 (LO), and E_2 (low) modes are described by Equation (6). Since Equation (6) contains two unknowns (σ_{xx} and E_z), the frequency shifts of two modes are sufficient to self-consistently measure both the in-plane stress and vertical electric field. Due to the low intensity of the E_2 (low) mode, most of the reports of micro-Raman thermography in the literature have used the E_2 (high) and A_1 (LO) modes to measure temperature rise and thermoelastic stress [4]-[6]. In this study, we also utilized the E_2 (high) and A_1 (LO) modes, which can be measured simultaneously without moving the grating position of the spectrograph, to determine the in-plane stress and vertical electric field according to Equation (6). Raman spectra were acquired at different drain bias points ($V_{ds} \geq 0$ V) in the pinched OFF state (V_{gs} = -5 V), and the changes in frequency of the phonon modes were determined by fitting a Voigt lineshape [33] to each peak

and calculating the change in peak position (centroid of the Voigt lineshape) relative to the V_{ds} = 0, V_{gs} = -5 V peak position. Because the gate bias was below the threshold voltage of V_{th} = -2.8 V measured for this device, the drain and gate leakage currents were both below 10 μA/mm, resulting in negligible temperature rise due to self-heating. We also measured the change in E_2 (low) mode peak position with increasing drain bias in a separate series of measurements because the E_2 (low) mode could not be observed at the same time as the E_2 (high) and A_1 (LO) modes without moving the grating position of the spectrograph. Changes in the E_2 (high), A_1 (LO), and E_2 (low) peak positions with increasing drain bias in the pinched OFF state are shown in Figure 5 up to V_{ds} = 50 V at a gate bias of V_{gs} = -5 V measured in the gate-drain access region adjacent to the drain contact of one of the center fingers. For the E_2 (high) mode, Raman spectra were recorded in the parallel $\bar{z}(yy)z$ and cross-polarized $\bar{z}(xy)z$ to investigate the possibility of asymmetric strain and stress in the c-plane [17],[34]. The error bars in the change in Raman peak positions in Figure 5 represent the standard deviation of multiple spectra acquired at each drain bias point. For reference, the E_2 (high), A_1 (LO), and E_2 (low) frequencies at V_{ds} = 0 V, V_{gs} = -5 V were measured to be 568.36 ± 0.01 cm^{-1}, 734.14 ± 0.01 cm^{-1}, and 143.74 ± 0.01 cm^{-1}, respectively.

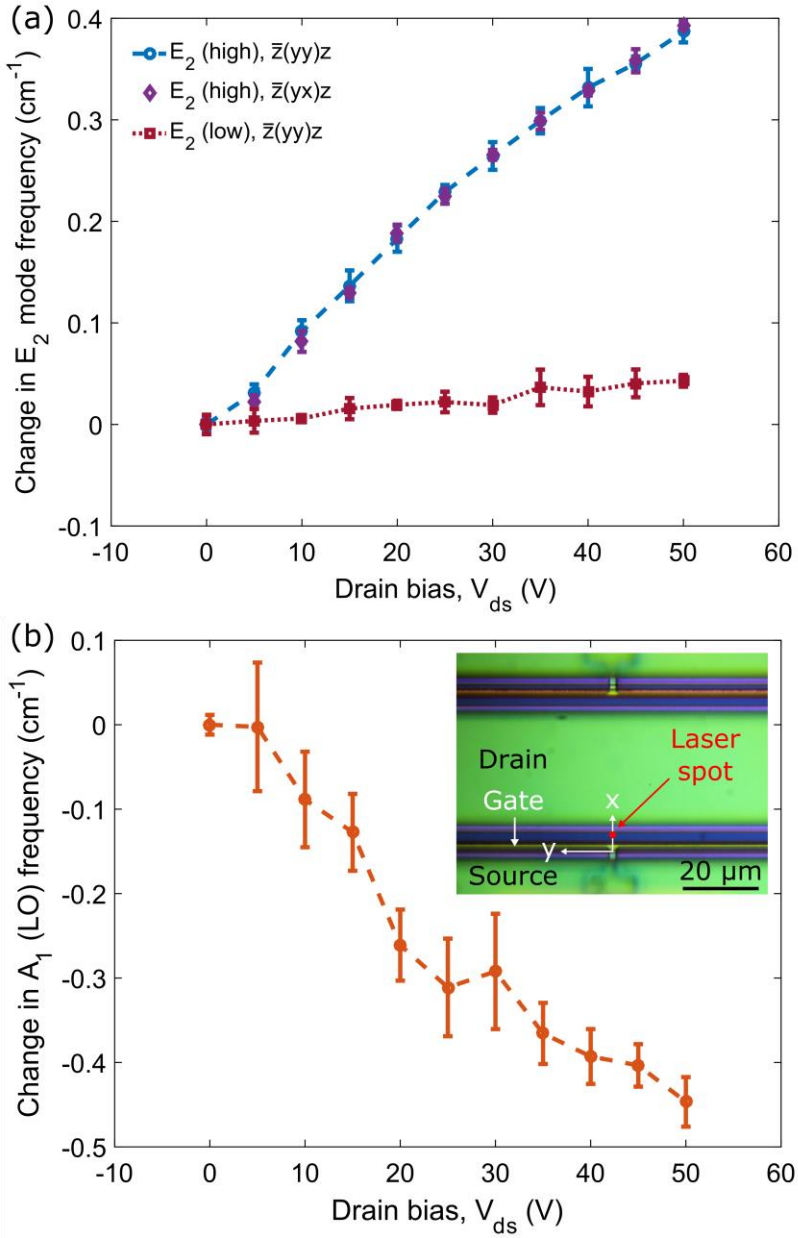

FIG. 5. (a) Change in E_2 (high) and E_2 (low) and (b) A_1 (LO) Raman peak positions with increasing drain bias in pinched OFF state adjacent to the drain contact in the gate-drain access region. Inset shows the device under test and measurement location. Error bars represent the standard deviation of multiple measurements taken at each drain bias.

As shown in Figure 5 and previously reported in the literature [3],[7]-[8], the E_2 (high) and A_1 (LO) peak positions shifted positively and negatively, respectively, when a positive drain bias was applied in the pinched OFF state. The magnitude of the A_1 (LO) peak shift was slightly higher

than that of the E_2 (high) peak, which has also been reported in previous studies. Within the error bars, we did not observe a difference in the change in Raman peak position of the E_2 (high) mode between measurements in the parallel and cross-polarized configurations, suggesting the asymmetry of the strain $\epsilon_{xx} - \epsilon_{yy}$ and stress $\sigma_{xx} - \sigma_{yy}$ in the c-plane does not exist or is too small to be measured [9]. We found that the E_2 (low) peak position also shifts positively by one order of magnitude less than the E_2 (high) mode (0.043 cm^{-1} vs. 0.39 cm^{-1} at V_{ds} = 50 V). Due to the frequency stabilized laser excitation, careful calibration of each Raman spectrum, and temperature stabilization of the sample, our measurements were repeatable to within the error bars.

IV. Electro-mechanical Modeling and Results

A. Electro-mechanical Device Model

In order to compare the values of strain, stress, and electric field related to the measured changes in Raman peak positions in Figure 5 and those expected in the GaN buffer for the device we tested, we developed a 3D uncoupled electro-mechanical model in the Silvaco ATLAS/BLAZE device simulation and COMSOL Multiphysics finite element software packages. First, we calculated the 2D electric potential with a semiconductor device model in Silvaco ATLAS/BLAZE; then, we determined the 3D electric field, stress, and strain distributions in the buffer in COMSOL Multiphysics from the electric potential from the previous step. More details of this electro-mechanical modeling framework can be found in our recent review [10]. In the Silvaco ATLAS/BLAZE model, we set the concentration of deep acceptor-type traps in the GaN buffer equal to a uniform value of 10^{17} cm^{-3} to account for the depletion region created in the gate-drain access region and under the drain contact when the drain is positively biased [8]-[9]. The sheet charge at the AlGaN/GaN interface was set to a value of 9×10^{12} cm^{-2} to reproduce the

threshold voltage of -2.8 V measured for this device at V_{ds} = 0.1 V. Careful attention was taken to model the geometry of the gate-connected and source-connected field plates from cross-sectional scanning electron microscopy images. The electric potential distribution in the device from the Silvaco ATLAS/BLAZE model is shown in Figure 6 for drain biases of V_{ds} = 0 V and 50 V at a gate bias of V_{gs} = -5 V. The difference between these two electric potential distributions is also plotted in Figure 6 because this difference corresponds to the measurement of $\Delta\omega = \omega(V_{ds} \geq 0) - \omega(V_{ds} = 0)$ used to experimentally determine the electric field, stress, and strain components.

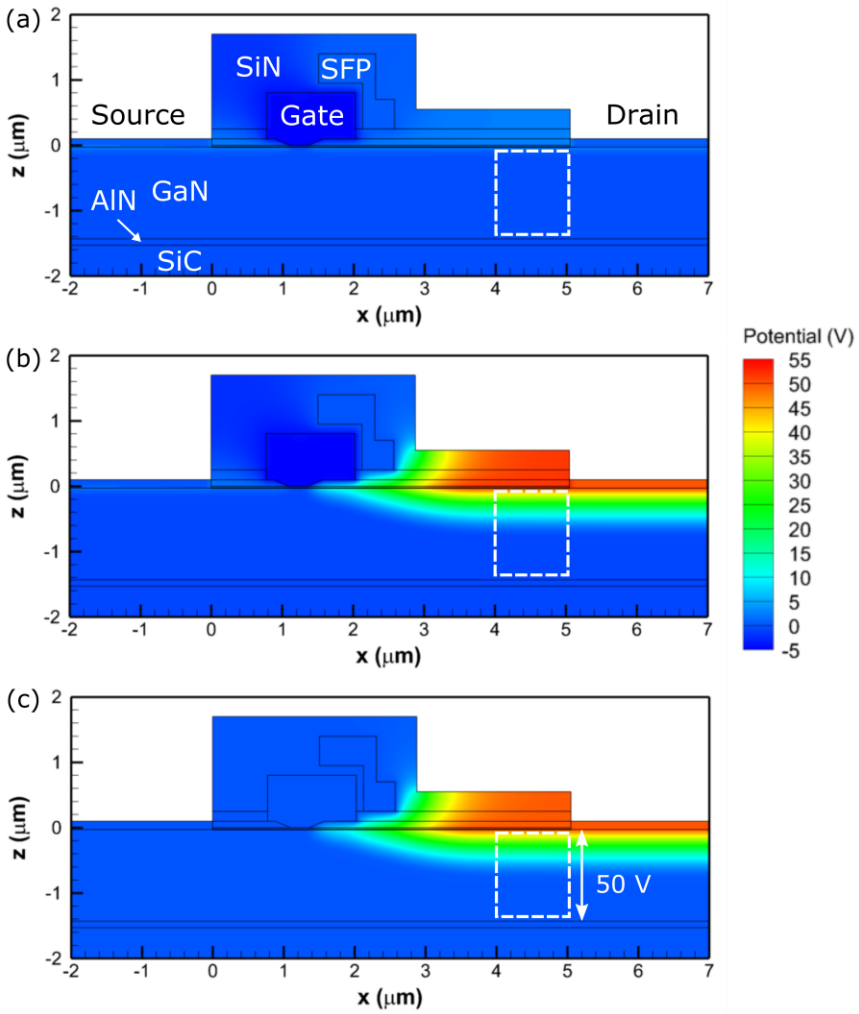

FIG. 6. Simulated electric potential distribution in the GaN-on-SiC HEMT in the pinched OFF state at (a) V_{ds} = 0 V and V_{gs} = -5 V and (b) V_{ds} = 50 V and V_{gs} = -5 V from the Silvaco ATLAS/BLAZE model. The difference between the potential distributions in (b) and (a) is plotted in (c) and is used as the input to the electro-mechanical model in COMSOL for comparison to the experimental results. The dashed region indicates the 1 μm diameter region where Raman spectra were measured in the experiments. "SiN" and "SFP" refer to the silicon nitride passivation layer and source connected field plate, respectively.

As seen in Figure 6, the application of a positive drain bias in the pinched OFF state results in a decreasing electric potential from the AlGaN barrier to the SiC substrate, which describes a negative electric field component E_z along the c-axis. The electric potential difference across the GaN buffer in Figure 6(c) is equal to the drain bias of 50 V so that the average vertical electric

field is equal to $\bar{E}_z = -V_{ds}/L_{buffer}$, where L_{buffer} is the thickness of the GaN buffer. There is also a lateral electric field component E_x along the channel but this field component is minimal next to the drain contact and only induces shear strain/stress in the xz plane, which should not affect the E_2 (high), A_1 (LO), and E_2 (low) frequencies to first-order [17]. The electric potential distribution in the GaN buffer (1.4 μm thick), AlN nucleation layer (100 nm thick), and SiC substrate (100 μm thick) calculated from the Silvaco ATLAS/BLAZE model was imported into COMSOL Multiphysics in order to calculate the electric field and solve for the mechanical stress and strain distributions shown in Figure 7. The top surface of the GaN buffer was allowed to freely deform (zero stress), the sides of the GaN buffer were assigned a symmetric displacement constraint (zero displacement along the x-direction), and the bottom of the substrate was set to zero displacement. As described in more detail by our prior work [10], these mechanical boundary conditions and the electric potential distribution in a GaN HEMT result in compressive strain along the c-axis ($\epsilon_{zz} < 0$), negligible strain in the c-plane ($|\epsilon_{xx}| \ll |\epsilon_{zz}|$), compressive stress in the c-plane ($\sigma_{xx} < 0$), negligible stress along the c-axis ($|\sigma_{zz}| \ll |\sigma_{xx}|$), and approximate symmetry in the c-plane ($\epsilon_{xx} \approx \epsilon_{yy}$ and $\sigma_{xx} \approx \sigma_{yy}$). Although there were significant spatial variations in the electric field, stress, and strain components throughout the buffer, the volumetric average values of these quantities are still related to each other through the constitutive relation in Equation (2).

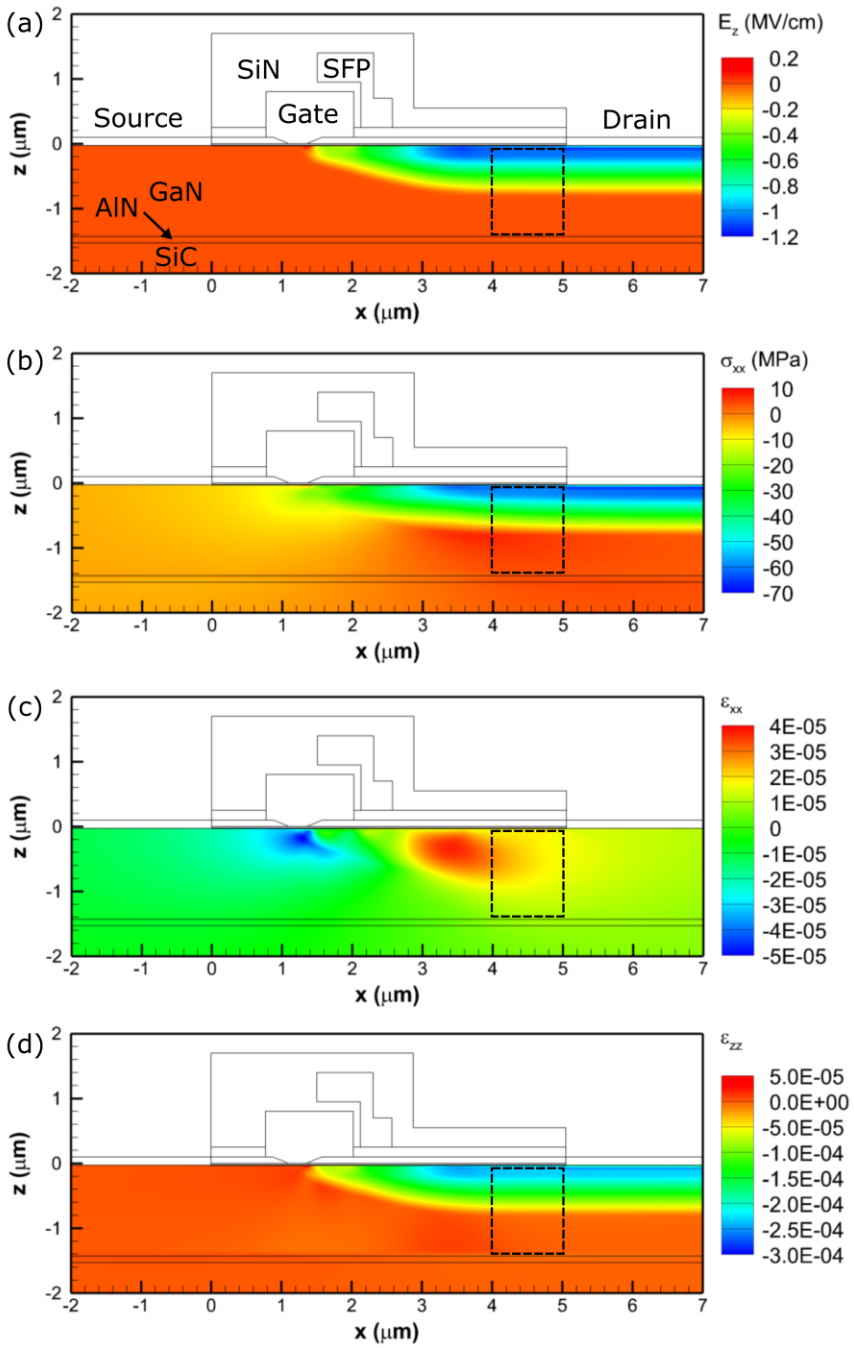

FIG. 7. (a) Vertical electric field E_z, (b) in-plane stress σ_{xx}, (c) in-plane strain ϵ_{xx}, and (d) out-of-plane strain ϵ_{zz} at the center of the gate calculated with the COMSOL Multiphysics model at V_{ds} = 50 V and V_{gs} = -5 V. The dashed region indicates the 1 μm diameter region where Raman spectra were measured in the experiments.

B. Analysis of the Experimental Data

Using Equation (6), the in-plane stress σ_{xx} and vertical electric field E_z can be determined self-consistently from the experimentally measured changes in Raman peak position of two modes, such as the E_2 (high) and A_1 (LO) modes

$$\begin{bmatrix}\sigma_{xx}\\ E_z\end{bmatrix} = \begin{bmatrix}K_{E_2}^{II} & B_{E_2}\\ K_{A_1}^{II} & B_{A_1}\end{bmatrix}^{-1}\begin{bmatrix}\Delta\omega_{E_2}\\ \Delta\omega_{A_1}\end{bmatrix} \tag{10}$$

with the values of the biaxial stress and electric field coefficients listed in Table I. Then, the in-plane strain ϵ_{xx} and out-of-plane strain ϵ_{zz} components can be expressed in terms of the frequency shifts of these two phonon modes by the constitutive relations in Equation (2) to yield

$$\begin{aligned}\begin{bmatrix}\epsilon_{xx}\\ \epsilon_{zz}\end{bmatrix} &= \begin{bmatrix}S_{11}+S_{12} & d_{31}\\ 2S_{13} & d_{33}\end{bmatrix}\begin{bmatrix}\sigma_{xx}\\ E_z\end{bmatrix}\\ &= \begin{bmatrix}S_{11}+S_{12} & d_{31}\\ 2S_{13} & d_{33}\end{bmatrix}\begin{bmatrix}K_{E_2}^{II} & B_{E_2}\\ K_{A_1}^{II} & B_{A_1}\end{bmatrix}^{-1}\begin{bmatrix}\Delta\omega_{E_2}\\ \Delta\omega_{A_1}\end{bmatrix}\end{aligned} \tag{11}$$

In Figure 8, we show a comparison between modeled and measured values of the in-plane strain, out-of-plane strain, in-plane stress and vertical electric field with increasing drain bias derived from the measured changes in the E_2 (high) and A_1 (LO) frequencies. To further support our hypothesis that the vertical electric field is shifting the phonon frequencies apart from the IPE effect, we also plotted the strain, stress, and electric field components derived from the E_2 (high) and E_2 (low) measurements shown in Figure 5 even though these peak shifts were not measured at the same time. Strain, stress, and electric field values from the electro-mechanical model shown in Figure 8 were calculated by averaging these quantities through the thickness of the 1.4 μm GaN buffer over a 1 μm region directly adjacent to the drain contact. While these quantities vary significantly through the thickness of the GaN buffer, the depth of field of ≈4 μm is larger than the

buffer thickness so that Raman scattering is collected from the entire buffer. Although it is possible that laser light absorption and other factors could result in non-uniform optical sampling of the buffer, we believe these factors have a negligible impact on the shift of the peak position derived from the aggregate Raman spectrum collected in the experiment [10]. The error bars in Figure 8 represent 95% confidence intervals on the measured values of the electric field, stress, and strain components determined from the variance in Raman peak position measured at each drain bias point, treating $\omega(V_{ds} \geq 0)$ and $\omega(V_{ds} = 0)$ as independent measurands. For simplicity, uncertainties in the phonon stress coefficients and elastic and piezoelectric constants were not included in the calculation of the confidence intervals.

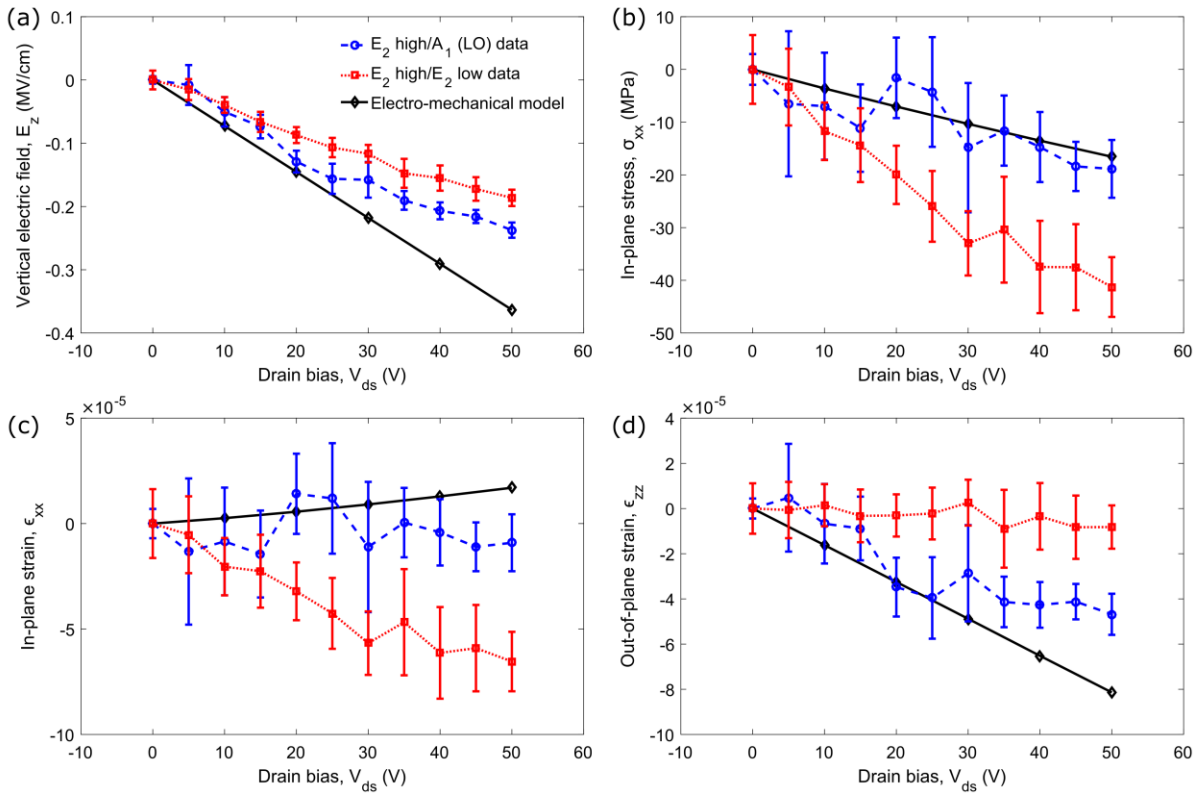

FIG. 8. Measured and modeled values of the (a) vertical electric field E_z, (b) in-plane stress σ_{xx}, (c) in-plane strain ϵ_{xx}, and (d) out-of-plane strain ϵ_{zz} and from analysis of the E_2 (high), A_1 (LO), and E_2 (low) Raman peak shifts. Values from the model in COMSOL Multiphysics represent depth-averaged values through the thickness of the GaN buffer. The error bars represent 95% confidence intervals on the measured values of the electric field, stress, and strain components determined from the variance in Raman peak position measured at each drain bias point

Using the measured E_2 (high) and A_1 (LO) peak shifts and the total electric field shift coefficient $B = B^{(i)} + B^{(ii+iii)}$ in Equation (6), our experimental data in Figure 8(a) shows that the average vertical electric field in the GaN buffer is negative and increases with drain bias in the pinched OFF state. The values of the vertical electric field derived from the experimental data are ≈35% lower in magnitude than those predicted by the electro-mechanical model, which are very close to $\bar{E}_z = -V_{ds}/L_{buffer}$. At a drain bias of 50 V, the average vertical electric field was measured to be -0.24 ± 0.01 MV/cm while the model predicted a value of -0.36 MV/cm. The in-

plane stress in Figure 8(b) was found to be compressive ($\sigma_{xx} < 0$) with a magnitude up to -19 ± 5 MPa at V_{ds} = 50 V and with good quantitative agreement between measured and modeled values. If we did not include the electric field coefficient $B^{(ii+iii)}$ in the analysis of the experimental data, we would have obtained values of 6.0 ± 0.3 MV/cm and -104 ± 4 MPa for the vertical electric field and in-plane stress at V_{ds} = 50 V, respectively, which deviate significantly from the modeled values. Owing to the fact that the bottom surface of the GaN buffer is clamped in the c-plane by the substrate but free to expand along the c-axis, our electro-mechanical model predicts that the in-plane strain (ϵ_{xx} = 1.7 × 10^{-5} at V_{ds} = 50 V) should be much less than the out-of-plane strain (ϵ_{zz} = -8.1 × 10^{-5} at V_{ds} = 50 V). From the E_2 (high)/A_1 (LO) experimental data, we found that the in-plane strain values plotted in Figure 8(c) are indeed less than the out-of-plane strain values, which noticeably increase with drain bias in Figure 8(d). Because the electric field coefficient apart from the IPE effect $B^{(ii+iii)}$ is an order of magnitude larger than that associated with the IPE effect $B^{(i)}$ for the E_2 (high) and A_1 (LO) modes, the phonon frequencies are much more sensitive to the vertical electric field than to the IPE-induced strain and stress components. As a result, uncertainties in the strain and stress components are relatively large compared to that of the vertical electric field.

We also found that the vertical electric field derived from the E_2 (high) and E_2 (low) mode measurements is negative but ≈25% lower in magnitude than the values obtained from the E_2 (high) and A_1 (LO) modes. The in-plane stress values showed a similar trend of increasing compressive stress with increasing drain bias but with values approximately twice as high as those predicted by the model and derived from the other phonon modes. Due to these differences in the in-plane stress and vertical electric field values, the in-plane and out-of-plane strain values obtained from the E_2 (high) and E_2 (low) modes displayed the opposite trends of those from the E_2

(high) and A_1 (LO) modes. We attribute these differences mainly to uncertainty in the biaxial stress coefficient of the E_2 (low) mode [29]-[30], which has not been measured by as many references as the E_2 (high) and A_1 (LO) modes [27],[29]-[30], and the general difficulty in measuring the small shifts of the E_2 (low) mode, e.g., -0.043 cm^{-1} at V_{ds} = 50 V. The E_2 (high) and A_1 (LO) modes provide a more reliable data set to determine quantitative values of the strain, stress, and electric field components but the E_2 (low) mode strengthens our hypothesis by providing an independent measurement of the vertical electric field.

Based on these results, we have developed a more complete understanding for the reason the pinched OFF state is the proper unpowered reference needed to decouple the effects of temperature rise and thermoelastic stress from those of IPE-induced stress and electric field on the Raman peak positions in the ON state in GaN HEMTs. Following Ref. [10] and the Appendix of this paper, the total change in Raman peak position of a single mode between the zero bias state and ON state is given by

$$\omega_{ON}(V_{ds} \geq 0) - \omega_0(V_{ds} = 0) = K^{II}\sigma_{xx} + BE_z^{ON} + A\Delta T \tag{12}$$

where the total in-plane stress $\sigma_{xx} = \sigma_{xx}^{TE} + \sigma_{xx}^{IPE}$ is the sum of the thermoelastic and IPE-induced contributions, the total electric field coefficient B includes the contributions of $B^{(i)}$ and $B^{(ii+iii)}$, and the total temperature coefficient A includes the contributions of thermoelastic strain and phonon-phonon coupling [6]. The total change in Raman peak position between the unpowered state OFF (V_{ds} = 0) state and the pinched OFF state ($V_{ds} \geq 0$) at the same subthreshold gate bias is given by

$$\omega_{OFF}(V_{ds} \geq 0) - \omega_{OFF}(V_{ds} = 0) = K^{II}\sigma_{xx}^{IPE} + BE_z^{OFF} \tag{13}$$

because there is negligible temperature rise and thermoelastic stress. Based on our previous finding [10] that the average vertical electric field in the GaN buffer is approximately the same for the same drain-gate bias ($V_{dg} = V_d - V_g$) associated with Equations (12) and (13), i.e., $E_z^{ON} \approx E_z^{OFF}$, we subtract Equation (13) from Equation (12) to yield

$$\omega_{ON}(V_{ds} \geq 0) - \omega_{OFF}(V_{ds} \geq 0) = K^{II}\sigma_{xx}^{TE} + A\Delta T \tag{14}$$

In deriving Equation (14), we have assumed that the IPE-induced stress σ_{xx}^{IPE} is the same in Equations (12) and (13) because the average vertical electric field is approximately the same. We have also assumed that the difference between the unpowered OFF state and zero bias state $\omega_{OFF}(V_{ds} = 0) - \omega_0(V_{ds} = 0) \approx 0$ because the gate bias has a very weak impact on the Raman peak positions at zero drain bias [8]. Thus, measuring the change in Raman peak position between the pinched OFF state and ON state at the same drain bias given by Equation (14) removes the impact of the IPE-induced stress and electric field on the Raman peak position.

V. Conclusions

In this work, we provided experimental evidence that the electric field can shift the optical phonon frequencies in wurtzite GaN apart from the IPE effect. Although this effect has been previously demonstrated via first principles calculations for zincblende GaAs, it has been overlooked in previous studies attempting to quantify the IPE-related strain and stress induced in the GaN buffer of HEMTs biased in the pinched OFF state. From our own first principles calculations, we found that the zone center optical phonon frequencies of the E_2 (high), A_1 (LO), and E_2 (low) modes are very strongly shifted by the electric field component along the c-axis, which we explain in terms of the change in the internal structural u parameter, even at zero macroscopic strain. Using measurements of the E_2 (high), A_1 (LO), and E_2 (low) phonon

frequencies obtained via micro-Raman spectroscopy in GaN HEMTs, we derived values of the dominant strain, stress, and vertical electric field components that are in good agreement with our 3D electro-mechanical model of the device. Apart from this specific application to GaN HEMTs, this work has a far greater significance in the lattice dynamics of piezoelectric semiconductors, which should all exhibit this effect. Further research, including direct measurement of the electric field coefficients, are needed to obtain better agreement between micro-Raman spectroscopy measurements and electro-mechanical modeling. Regardless, this work represents a significant advance in our understanding of the electro-mechanical state of the GaN buffer under bias and the reason the pinched OFF state acts as the proper reference for micro-Raman thermography, decoupling the temperature rise and thermoelastic stress from the electric field and the IPE-induced stress.

Acknowledgements

The authors would like to thank Mr. Sameer Joglekar, Mr. Daniel Piedra, Dr. Omair I. Saadat, and Prof. Tomás Palacios of the Department of Electrical Engineering and Computer Science at the Massachusetts Institute of Technology (MIT) for providing GaN devices used at the early stages of this study and assisting with device characterization. The authors would also like to thank Mr. Vazrik Chiloyan of the Department of Mechanical Engineering at MIT and Dr. James Fiorenza of Analog Devices, Inc. for helpful technical discussions. K. R. Bagnall and E. N. Wang acknowledge funding support provided by the MIT/MTL GaN Energy Initiative and MIT-Singapore SMART LEES Program. K. R. Bagnall also acknowledges that this research was conducted with Government support under and awarded by DoD, Air Force Office of Scientific Research, National Defense Science and Engineering Graduate (NDSEG) Fellowship, 32 CFR 168a. D. Vanderbilt and C. E. Dreyer acknowledge support from ONR grant N00014-12-1-1035.

Experimentally facilities were graciously provided by Prof. Jing Kong of the Department of Electrical Engineering and Computer Science at MIT and the MIT Laser Biomedical Research Group and by the MIT Institute for Soldier Nanotechnologies (ISN) at the early stages of this study.

Appendix: Derivation of the Phonon Frequency Shift with Strain, Stress, Electric Field, and Temperature

Optical phonon frequencies near the Γ-point of wurtzite GaN, which we characterized by micro-Raman spectroscopy, are simultaneously affected by strain, stress, electric field, and temperature rise in GaN HEMTs. Fundamental studies in the literature on the temperature dependence of phonon-phonon interactions [35], the stress dependence of optical phonon frequencies (piezospectroscopy) [17],[19], and the electric field dependence of phonon frequencies [18]-[19] have considered each of these factors in isolation. To the best of our knowledge, there has not been a comprehensive theoretical treatment supporting Equation (12) that combines the effect of these four factors in a self-consistent manner. Previous experimental works in micro-Raman thermography of GaN HEMTs [4]-[10],[11] have indirectly suggested that Equation (12) is valid by empirically assessing the impact of stress, electric field, and temperature on the Raman spectrum of wurtzite GaN. In this appendix, we derive the full form of Equation (12) from potential deformation theory [17], which simplifies to Equation (6) when there is zero temperature rise.

As discussed in Section II, the standard formalism of potential deformation theory from piezospectroscopy [17] assumes that the crystal potential is slightly perturbed under an applied strain, which can be expanded linearly in terms of the strain components. First-order perturbation theory is then used to determine the shifts of the energy eigenvalues or frequencies of the phonon modes by evaluating matrix elements of the form $\langle \phi_n | V_{ij} | \phi_m \rangle$, where $|\phi_m\rangle$ is the unperturbed

eigenfunction of a particular mode and V_{ij} is the perturbation operator associated with the strain component ϵ_{ij}. Symmetry analysis (group theory) determines whether a particular matrix element $\langle\phi_n|V_{ij}|\phi_m\rangle$ vanishes owing to the symmetry of the modes and that of the perturbation V_{ij}. In Section II, we argued that the strain perturbation should be augmented by another term that accounts for the perturbation to the crystal potential from an electric field that is independent of the strain induced by the IPE effect. In other words, if the primitive unit cell of crystal is perfectly constrained by mechanical forces in the presence of a non-zero macroscopic electric field, a perturbation term expanded only in terms of the strain components suggests that there should be no change in the phonon frequencies. However, we found from first principles calculations that an electric field along the c-axis strongly shifts the internal structural u parameter and optical phonon frequencies of wurtzite GaN, even at fixed values of the lattice parameters a and c (zero macroscopic strain). Therefore, we added an additional term appearing in Equation (5) that led to the presence of the electric field coefficient $B^{(ii+iii)}$ in Equation (6), which is independent of the IPE effect. The need for this additional term is also consistent with the principle that two intrinsic properties (strain, stress, polarization, and electric field) are required to specify the thermodynamic state and structure of a piezoelectric crystal.

As seen in expression for the free energy of a piezoelectric and thermoelastic crystal

$$d\Phi = \sigma_{ij} d\epsilon_{ij} - P_i dE_i - Tds \tag{A1}$$

where Φ is the specific free energy, P_i is the polarization vector, and s is the specific entropy, the thermodynamic state of the crystal is determined by the temperature and the specific entropy in addition to the strain, stress, electric field, and polarization. Therefore, we must also augment the perturbation to the crystal potential by a term that depends on temperature to account for the

contribution of the temperature change to the perturbation of the crystal potential apart from thermoelastic strain, i.e.,

$$V = \sum_{ij} V_{ij}^{(i)} \epsilon_{ij} + \sum_{k} V_{k}^{(ii+iii)} E_k + V^{(iv)} \Delta T \tag{A2}$$

The physical origin of this contribution $V^{(iv)}$ to the crystal potential is the influence of the ensemble of phonon modes at a finite temperature T to the frequency of a particular mode due to anharmonic phonon-phonon interactions [35]. By examining the character table of the point group C_{6v} [36] reproduced in Table II, we can describe the symmetry properties of the terms appearing in Equation (A2) as $\Gamma^{(i)} = 2A_1 + E_1 + E_2$, $\Gamma^{(ii+iii)} = A_1 + E_1$, and $\Gamma^{(iv)} = A_1$ because these three terms transform as a second-order tensor, a polar vector, and a scalar, respectively.

TABLE II. Character table for the point group C_{6v} [36].

			E	C_2	$2C_3$	$2C_6$	$3\sigma_d$	$3\sigma_v$
x^2+y^2, z^2	z	A_1	1	1	1	1	1	1
		A_2	1	1	1	1	-1	-1
		B_1	1	-1	1	-1	-1	1
		B_2	1	-1	1	-1	1	-1
(xz, yz)	(x, y)	E_1	2	-2	-1	1	0	0
(x^2-y^2, xy)		E_2	2	2	-1	-1	0	0

From first-order perturbation theory, the energy shift of the A_1 (LO) mode in wurtzite GaN due to strain, electric field, and temperature is related to the matrix elements $\langle \phi_{A_1} | V | \phi_{A_1} \rangle$ [37], many of which may vanish due to symmetry. This can be determined by evaluating the direct product of the representations of the phonon mode $\Gamma_{phonon} = A_1$ and that of the perturbation $\Gamma_V = 4A_1 + 2E_1 + E_2$ according to $\Gamma_V \otimes \Gamma_{phonon}$. If this direct product does not contain the representation of the mode Γ_{phonon}, then particular matrix elements $\langle \phi_{A_1} | V | \phi_{A_1} \rangle$ vanish and

certain strain, electric field, and/or temperature rise components have no effect on the optical phonon frequencies [36]. In the simple case of the A_1 (LO) mode, only the terms transforming as A_1 in Γ_V contribute to the energy shift of the A_1 mode, which we write in terms of the frequency as

$$\Delta\omega_{A_1} = a_{A_1}\left(\epsilon_{xx} + \epsilon_{yy}\right) + b_{A_1}\epsilon_{zz} + B_{A_1}^{(ii+iii)}E_z + A_{A_1}^{(iv)}\Delta T \tag{A3}$$

where $A_{A_1}^{(iv)}$ is the temperature coefficient of the A_1 (LO) mode apart from thermoelastic strain. Using the constitutive relation for a piezoelectric and thermoelastic solid, we can rewrite Equation (A3) in terms of the stress, electric field, and temperature as

$$\Delta\omega_{A_1} = \tilde{a}_{A_1}\left(\sigma_{xx} + \sigma_{yy}\right) + \tilde{b}_{A_1}\sigma_{zz} + \left[B_{A_1}^{(i)} + B_{A_1}^{(ii+iii)}\right]E_z + \left[A_{A_1}^{(i)} + A_{A_1}^{(iv)}\right]\Delta T \tag{A4}$$

where the $\tilde{a}_{A_1} = \frac{1}{2}K_{A_1}^{II} = a_{A_1}(S_{11} + S_{12}) + b_{A_1}S_{13}$ is the uniaxial stress coefficient in the c-plane [10],[27], $\tilde{b}_{A_1} = 2a_{A_1}S_{13} + b_{A_1}S_{33}$ is the uniaxial stress coefficient along the c-axis [29], $B_{A_1}^{(i)} = 2a_{A_1}d_{31} + b_{A_1}d_{33}$ is the IPE strain-related electric field coefficient [10], and $A_{A_1}^{(i)} = 2a_{A_1}\alpha_{xx} + b_{A_1}\alpha_{zz}$ is the thermoelastic strain-related temperature coefficient. This is a general form of Equation (12) that accounts for all of the first-order contributions of strain, stress, electric field, and temperature to the frequency shift of the A_1 (LO) mode in wurtzite GaN.

For the E_2 (high) and E_2 (low) modes, the corresponding calculation is slightly more complicated because the modes transforming as E_2 are doubly degenerate, i.e., there are two modes labeled as E_2 (high) with the same frequency that represent atoms vibrating along the x- and y-axes, respectively. In this case, degenerate first-order perturbation theory specifies that the energy shift of the E_2 (high) mode is given by the solution to the secular equation $|V_{k\ell} - \Delta\omega\delta_{k\ell}| = 0$, where $V_{k\ell} = \langle\phi_\ell|V|\phi_k\rangle$ and $\delta_{k\ell}$ is the Kroenicker delta tensor [37]. Only the matrix elements

$\langle \phi_{E_2(\ell)}|V|\phi_{E_2(k)}\rangle$ that do not vanish corresponding to terms in the direct product $\Gamma_V \otimes E_2$ that contain E_2 enter into the secular equation. After solving the secular equation, we found that the frequency shifts of the E_2 (high) and E_2 (low) modes are identical to that of the A_1 (LO) mode except for a term related to the asymmetric strain in the xy-plane [17]

$$\Delta\omega_{E_2} = a_{E_2}(\epsilon_{xx} + \epsilon_{yy}) + b_{E_2}\epsilon_{zz} \pm c_{E_2}\sqrt{(\epsilon_{xx} - \epsilon_{yy})^2 + 4\epsilon_{xy}^2} + B_{E_2}^{(ii+iii)}E_z + A_{E_2}^{(iv)}\Delta T \quad \text{(A5)}$$

All of the terms transforming as E_1 in the representation of the perturbation Γ_V (ϵ_{xz}, ϵ_{yz}, E_x, and E_y) do not affect the E_2 (high), A_1 (LO), and E_2 (low) modes to first-order. Equation (A5) can similarly be rewritten in terms of the stress, electric field, and temperature rise as

$$\Delta\omega_{E_2} = \tilde{a}_{E_2}(\sigma_{xx} + \sigma_{yy}) + \tilde{b}_{E_2}\sigma_{zz} \pm \tilde{c}_{E_2}\sqrt{(\sigma_{xx} - \sigma_{yy})^2 + 4\sigma_{xy}^2} + \left[B_{E_2}^{(i)} + B_{E_2}^{(ii+iii)}\right]E_z + \left[A_{E_2}^{(i)} + A_{E_2}^{(iv)}\right]\Delta T \quad \text{(A6)}$$

where $\tilde{c}_{E_2} = c_{E_2}|S_{11} - S_{12}|$ is the shear stress coefficient in the c-plane [17]. This derivation is consistent with potential deformation theory and identifies the individual mechanisms associated with stress, electric field, and temperature that contribute to the total frequency shift of the optical phonon modes.

References

[1] S. Chowdhury and U. K. Mishra, IEEE Trans. Electron Devices **60**, 3060 (2013).

[2] Y.-F. Wu, M. Moore, A. Saxler, T. Wisleder and P. Parikh in *Proceedings of the 64th Device Research Conference*, State College, PA, USA 26 June-28 June 2006 (IEEE, 2006), pp. 151-152.

[3] M. Kuball, J. M. Hayes, M. J. Uren, T. Martin, J. C. H. Birbeck, R. S. Balmer and B. T. Hughes, IEEE Electron Device Lett. **23**, 7 (2002).

[4] T. Beechem, A. Christiensen, S. Graham, and D. Green, J. Appl. Phys **103**, 124501 (2008).

[5] T. Batten, J. W. Pomeroy, M. J. Uren, T. Martin, and M. Kuball, J. Appl. Phys. **106**, 094509 (2009).

[6] S. Choi, E. R. Heller, D. Dorsey, R. Vetury, and S. Graham, IEEE Trans. Electron Devices **60**, 1898 (2013).

[7] G. J. Riedel, J. W. Pomeroy, K. P. Hilton, J. O. Maclean, D. J. Wallis, M. J. Uren, T. Martin, and M. Kuball, IEEE Electron Device Lett. **29**, 416 (2008).
[8] A. Sarua, H. Ji, M. Kuball, M. J. Uren, T. Martin, K. J. Nash, K. P. Hilton and R. S. Balmer, Appl. Phys. Lett. **88**, 103502 (2006).
[9] A. Sarua, H. Ji, J. W. Pomeroy, M. J. Uren, T. Martin and M. Kuball, Semicond. Sci. Technol. **25**, 085004 (2010).
[10] K. R. Bagnall and E. N. Wang, "Experimental characterization of inverse piezoelectric strain in GaN HEMTs via micro-Raman spectroscopy," **87**, 061501 (2016).
[11] T. Beechem, A. Christensen, D. S. Green, and S. Graham, J. Appl. Phys. **106**, 114509 (2009).
[12] O. Ambacher, J. Smart, J. R. Shealy, N. G. Weimann, K. Chu, M. Murphy, W. J. Schaff, L. F. Eastman, R. Dimitrov, L. Wittmer, M. Stutzmann, W. Rieger and J. Hilsenbeck, J. Appl. Phys. **85**, 3222 (1999).
[13] K. Momma and F. Izumi, J. Appl. Crystallogr. **44**, 1272 (2011).
[14] J. F. Nye, *Physical Properties of Crystals: Their Representation by Tensors and Matrices* (Oxford University Press, London, 1957), pp. 181-183, 300.
[15] C. A. Arguello, D. L. Rousseau and S. P. S. Porto, Phys. Rev. **181**, 1351 (1969).
[16] E. B. Saloman and C. J. Sansonetti, J. Phys. Chem. Ref. Data **33**, 1113 (2004).
[17] R. J. Briggs and A. K. Ramdas, Phys. Rev. B **13**, 5518 (1974).
[18] X. Wang and D. Vanderbilt, Phys. Rev. B **74**, 054304 (2006).
[19] S. Ganesan, A. A. Maradudin, and J. Oitmaa, Ann. Phys. **56**, 556 (1970).
[20] J. Heyd, G. E. Scuseria, and M. Ernzerhof, J. Chem. Phys. **118**, 8207 (2003). **124**, 219906 (2006).
[21] G. Kresse and J. Furthmuller, Phys. Rev. B **54**, 11169 (1996).
[22] P. E. Blochl, Phys. Rev. B **50**, 17953 (1994).
[23] H. J. Monkhorst and J. D. Pack, Phys. Rev. B **13**, 5188 (1976).
[24] A. Togo and I. Tanaka, Scr. Mater. **108**, 1 (2015).
[25] N. Sai, K. M. Rabe, and D. Vanderbilt, Phys. Rev. B **66**, 104108 (2002).
[26] X. Gonze, B. Amadon, P.M. Anglade, J.-M. Beuken, F. Bottin, P. Boulanger, F. Bruneval, D. Caliste, R. Caracas, M. Cote, T. Deutsch, L. Genovese, Ph. Ghosez, M. Giantomassi, S. Goedecker, D. Hamann, P. Hermet, F. Jollet, G. Jomard, S. Leroux, M. Mancini, S. Mazevet, M.J.T. Oliveira, G. Onida, Y. Pouillon, T. Rangel, G.-M. Rignanese, D. Sangalli, R. Shaltaf, M. Torrent, M.J. Verstraete, G. Zérah, J.W. Zwanziger. Computer Phys. Comm. 180, 2582-2615 (2009).
[27] S. Choi, E. Heller, D. Dorsey, R. Vetury, and S. Graham J. Appl. Phys. **113**, 093510 (2013).
[28] P. Witczak, Z. Witczak, R. Jemielniak, M. Krysko, S. Krukowski and M. Bockowski, Semicond. Sci. Technol. **30**, 1 (2015).
[29] A. R. Goñi, H. Siegle, K. Syassen, C. Thomsen and J.-M. Wagner, Phys. Rev. B **64**, 035205 (2001).
[30] G. Callsen, J. S. Reparaz, and M. R. Wagner, R. Kirste, C. Nenstiel, A. Hoffman and M. R. Phillips, Appl. Phys. Lett. **98**, 061906 (2011).
[31] R. S. Pengelly, S. M. Wood, J. W. Milligan, S. T. Sheppard, and W. L. Pribble, IEEE Trans. Microwave Theory Techniques **60**, 1764 (2012).
[32] N. J. Everall, Appl. Spectrosc. **63**, 245 (2009).
[33] Y. Liu and J. Lin, J. Opt. Soc. Am. B **18**, 666 (2001).

[34] V. Darakchieva, T. Paskova, M. Schubert, H. Arwin, P. P. Paskov, B. Monemar, D. Hommel, M. Heuken, J. Off, F. Scholz, B. A. Haskell, P. T. Fini, J. S. Speck and S. Nakamura, Phys. Rev. B **75**, 195217 (2007).
[35] J. Menendez and M. Cardona, Phys. Rev. B **29**, 2051 (1984).
[36] M. S. Dresselhaus, G. Dresselhaus, and A. Jorio, *Group Theory: Application to the Physics of Condensed Matter* (Springer-Verlag, Berlin, 2008), pp. 105-106, 483.
[37] J. J. Sakurai and J. Napolitano, *Modern Quantum Mechanics*, 2nd ed. (Addison-Wesley, San Francisco, 2011), pp. 308, 317-318.